Triplet absorption spectroscopy and electromagnetically induced transparency

2016 J. Phys. B: At. Mol. Opt. Phys. 49 175502

(http://iopscience.iop.org/0953-4075/49/17/175502)

IOP Publishing Journal of Physics B: Atomic, Molecular and Optical Physics
J. Phys. B: At. Mol. Opt. Phys. **49** (2016) 175502 (11pp) doi:10.1088/0953-4075/49/17/175502

Triplet absorption spectroscopy and electromagnetically induced transparency

F Ghafoor[1,4] **and R G Nazmitdinov**[2,3]

[1] Department of Physics, COMSATS Institute of Information Technology, Islamabad, Pakistan
[2] Departament de Física, Universitat de les Illes Balears, E-07122 Palma de Mallorca, Spain
[3] Bogoliubov Laboratory of Theoretical Physics, Joint Institute for Nuclear Research, 141980 Dubna, Russia

E-mail: rishteen@yahoo.com

Received 17 February 2016, revised 30 May 2016
Accepted for publication 18 July 2016
Published 15 August 2016

Abstract

Coherence phenomena in a four-level atomic system, cyclically driven by three coherent fields, are investigated thoroughly at zero and weak magnetic fields. Each strongly interacting atomic state is converted to a triplet due to a dynamical Stark effect. Two dark lines with a Fano-like profile arise in the triplet absorption spectrum with anomalous dispersions. We provide conditions to control the widths of the transparency windows by means of the relative phase of the driving fields and the intensity of the microwave field, which closes the optical system loop. The effect of Doppler broadening on the results of the triplet absorption spectroscopy is analysed in detail.

Keywords: Autler–Townes spectroscopy, Fano resonances and switching, triplet absorption spectroscopy, electromagnetically induced transparency, slow and fast light

(Some figures may appear in colour only in the online journal)

1. Introduction

The absorption spectrum of a two-level atomic system exhibits a Lorentzian line shape in the absence of any driving field [1]. The spectrum is modified when the excited state is coupled to another excited state by a strong laser field. As a result, each excited state splits on two components. This is the so-called Autler–Townes (AT) doublet [2–4], which has been extensively studied in the context of spontaneous emission spectra [5–7], stimulated absorption [8–12], and wave mixing [13–16], to name just a few. Indeed, the doublets appear in various three-level atomic or molecular systems interacting with a strong laser field [17]. In the absorption spectra of such systems a dark line appears in the probe excitation signal under the ideal conditions. That dark line, which is the essence of electromagnetically induced transparency (EIT) [17, 18], is due to a quantum interference between two alternative indistinguishable transition pathways created by the coupling fields with the internal states of a quantum system. The EIT is also a manifestation of Fano-like interference. This interference is characterized by an asymmetric line shape of the resonance spectrum, which is created by various mechanisms in different quantum systems [19]. In particular, this asymmetric line shape of resonances has been predicted in atomic ionization due to a laser-induced continuum structure (for a review see [20]). The possibility of altering losses of optical beams by strong laser fields attracts researches to employ EIT-based schemes, for example, to slow the group velocity of a sub-luminal optical probe pulse transmitted by optical media (for a review see [21]).

The phenomenon of AT doublet absorption spectroscopy can be further generalized when a multi-level atom is considered. It is expected that Fano-like interference will be present in this case as well. Evidently, the multiplicative action of these mechanisms in multi-level atoms under strong laser fields opens a new avenue to explore various aspects of the absorption cancellation absent in AT doublet spectroscopy. In fact, the connection of triplet spectroscopy with EIT presents a real challenge to the field of atomic spectroscopy [22]. Note that the ability to control, for example, the properties of double EIT (which is absent in the case of three-level systems)—two transparency windows convert to one and

[4] Author to whom any correspondence should be addressed.

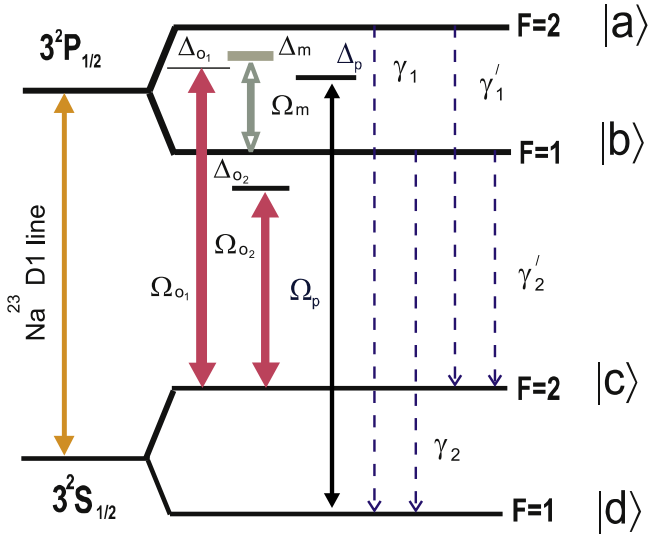

Figure 1. A sketch of the atomic energy spectrum of the sodium D1 line at zero magnetic field.

vice versa—may be used as an optical switcher in nanophotonics.

To elucidate the typical features of triplet absorption spectroscopy we consider four-level atomic schemes with different radiative decay mechanisms, cyclically driven by three coherent fields. In addition, our systems interact with the microwave field whose frequency is much smaller than those of the optical fields. It will be shown that the variation of the intensities and phases of optical and microwave fields enables one to control the degree of super- and sub-luminality in the transparency windows in absorption triplet spectroscopy. The influence of Doppler broadening, important from the experimental point of view, will be taken into account in our consideration. In this case the mismatch of the optical and microwave frequencies will be analysed thoroughly.

The structure of the paper is as follows. In section 2 we introduce our model. The Doppler broadening and the vector mismatch are highlighted here as well. In section 3 we discuss various aspects of triplet absorption spectroscopy, when there are multiple decay channels. Section 4 is devoted to the analysis of triplet absorption spectroscopy, when there is only one decay channel. The main conclusions are summarized in section 5.

2. The model

2.1. Stationary electrical susceptibility

As a typical example of an atomic system interacting with optical fields, we consider first an atomic scheme similar to the Na^{23} D1 line ($3S^2_{1/2} \Longleftrightarrow 3P^2_{1/2}$) with $\lambda = 5895.93$Å at nonzero spin–orbit interaction and zero magnetic field (see figure 1). Levels $3^2P_{1/2}$, $F = 2$ ($|a\rangle$), and $3^2P_{1/2}$, $F = 1$ ($|b\rangle$), of the excited doublet are driven by a microwave field with the Rabi frequency Ω_m. These closely spaced levels are coupled with the ground state $3\ ^2S_{1/2}$, $F = 2$ ($|c\rangle$), by means of two coherent optical fields with the Rabi frequencies Ω_{o_1} and Ω_{o_2}.

Excited states decay to the lowest ground state, $3^2S_{1/2}$, $F = 2$ ($|c\rangle$), and $3^2S_{1/2}$, $F = 1$ ($|d\rangle$), by means of allowed electric dipole transitions. A weak probe field (with the Rabi frequency Ω_p) couples the lowest ground state $|d\rangle$ and the excited state $|a\rangle$. We define the optical field detuning parameters as: $\Delta_{o_1} = \omega_{ca} - \omega_{o_1}$, $\Delta_{o_2} = \omega_{cb} - \omega_{o_2}$. The detuning parameters of the microwave and probe fields are $\Delta_m = \omega_{ba} - \omega_m$, and $\Delta_p = \omega_{da} - \omega_p$, respectively. Here, the frequencies ω_{o_1,o_2} are associated with two optical fields: ω_m corresponds to the microwave field, while the frequency ω_p characterises the probe field.

In general, the Rabi frequencies can be complex $\Omega_i = |\Omega_i|\exp(i\phi_i)$, $i = o_1, o_2, m, p$. For the sake of simplicity, we consider the phase associated with the probe field to be fixed as $\phi_p = 0$. Below, for the sake of convenience, we omit the modulus, i.e. $|\Omega_i| \Rightarrow \Omega_i$.

The response of a medium due to interaction of these fields with the atomic system under consideration can be found with the aid of the susceptibility of the system (see for details [1])

$$\chi = \frac{N\wp_{ad}}{\epsilon_0 E}\rho_{ad}. \tag{1}$$

Here, $\wp_{ad}$ is a dipole matrix element, N is the number density of gas atoms, and ρ_{ad} is the density matrix element between states $|a\rangle$ and $|d\rangle$.

To trace a dynamical behaviour of the probe pulse in the medium we need to evaluate the group index for our system. It is related to the group velocity v_g via $N_g = c/v_g$, where c is the speed of light in a vacuum. The group index is calculated as:

$$N_g = 1 + 2\pi\,\mathrm{Re}[\chi] + 2\pi\omega_{ad}\,\mathrm{Re}\left[\frac{\partial\chi}{\partial\Delta_p}\right]. \tag{2}$$

Thus, to analyse the response of our systems to external fields, we have to know the time evolution of the density matrix ρ_{ad}. To solve that problem we employ the master equation in Lindblad form

$$\frac{\mathrm{d}\rho}{\mathrm{d}t} = -\frac{\mathrm{i}}{\hbar}[H_I, \rho] + \Lambda\rho, \tag{3}$$

with a damping term:

$$\Lambda\rho = -\frac{1}{2}\Gamma\sum(\sigma^\dagger\sigma\rho + \rho\sigma^\dagger\sigma - 2\sigma\rho\sigma^\dagger). \tag{4}$$

Here $\sigma = |a\rangle\langle d|$ or $|b\rangle\langle d|$ and $\sigma^\dagger = |d\rangle\langle a|$ or $|d\rangle\langle b|$ are the lowering and raising operators for the two decay transitions of the system, respectively. In particular, for the spontaneous decay rate of the excited state $3^2P_{3/2} \rightarrow 3^2S_{1/2}$ one has

$$\Gamma = \frac{1}{4\pi\varepsilon_0}\frac{4|\wp_{ad}|^2\omega_{da}^3}{3\hbar c^3} \equiv \gamma. \tag{5}$$

Our system is described by the Hamiltonian, taken in the interaction representation and in the rotating wave

approximation (for details of the derivation, see, for example, [1]):

$$H_I = -\frac{\hbar}{2}[\Omega_m e^{i(\Delta_m t+\varphi_m)}|a\rangle\langle b| + \Omega_{o_1} e^{i(\Delta_{o_1} t+\varphi_{o_1})}|a\rangle\langle c| + \Omega_{o_2} e^{i(\Delta_{o_2} t+\varphi_{o_2})}|b\rangle\langle c| + \Omega_p e^{i\Delta_p t}|a\rangle\langle d|] + \text{H.c.} \quad (6)$$

To proceed further, we use the transformations

$$\begin{aligned} \rho_{ad} &\to \tilde{\rho}_{ad} e^{i\Delta_p t}, \\ \rho_{cd} &\to \tilde{\rho}_{cd} e^{-i(\Delta_{o_1}-\Delta_p)t}, \\ \rho_{bd} &\to \tilde{\rho}_{bd} e^{-i(\Delta_m-\Delta_p)t}, \\ \rho_{ba} &\to \tilde{\rho}_{ba} e^{-i\Delta_m t}, \\ \rho_{cd} &\to \tilde{\rho}_{cd} e^{-i\Delta_{o_1} t}. \end{aligned} \quad (7)$$

By means of (3) and (4), in virtue of transformation (7), one obtains the following three coupled rate equations for slowly varying amplitudes (in the first order of the probe field and all orders of the coherent driving fields)

$$\frac{d\tilde{\rho}_{ad}}{dt} = -\left[i\Delta_p + \frac{1}{2}(\gamma_1+\gamma_1')\right]\tilde{\rho}_{ad} + \frac{i}{2}\Omega_m e^{i\varphi_m}\tilde{\rho}_{bd} + \frac{i}{2}\Omega_{o_1} e^{i\varphi_{o_1}}\tilde{\rho}_{cd} - \frac{i}{2}\Omega_p(\tilde{\rho}_{aa}-\tilde{\rho}_{dd}), \quad (8)$$

$$\frac{d\tilde{\rho}_{bd}}{dt} = -\left[i(\Delta_p-\Delta_m) + \frac{1}{2}(\gamma_2+\gamma_2')\right]\tilde{\rho}_{bd} + \frac{i}{2}\Omega_m^{\star} e^{-i\varphi_m}\tilde{\rho}_{ad} + \frac{i}{2}\Omega_{o_2} e^{i\varphi_{o_2}}\tilde{\rho}_{cd} - \frac{i}{2}\Omega_p\tilde{\rho}_{ba}, \quad (9)$$

$$\frac{d\tilde{\rho}_{cd}}{dt} = -i(\Delta_p-\Delta_{o_1})\tilde{\rho}_{cd} + \frac{i}{2}\Omega_{o_1} e^{i\varphi_{o_1}}\tilde{\rho}_{ad} + \frac{i}{2}\Omega_{o_2} e^{i\varphi_{o_2}}\tilde{\rho}_{bd} - \frac{i}{2}\Omega_p\tilde{\rho}_{ca}. \quad (10)$$

It is natural to employ the following initial state conditions: $\tilde{\rho}_{dd}=1, \tilde{\rho}_{aa}=0, \tilde{\rho}_{ba}=0, \tilde{\rho}_{ca}=0$. The above set of equations can be solved for $\tilde{\rho}_{ad}$ with the aid of the equation

$$R(t) = \int_{-\infty}^{t} e^{-Q(t-t')}P dt' = Q^{-1}P, \quad (11)$$

where $R(t)$ and P are column matrices, while Q is a 3×3 matrix.

The solution is:

$$\tilde{\rho}_{ad} = -\text{Re}[\tilde{\rho}_{ad}] - i\,\text{Im}[\tilde{\rho}_{ad}] \quad (12)$$

with

$$\text{Re}[\tilde{\rho}_{ad}] = \frac{2(\gamma_2+\gamma_2')B_G(\Delta_{o_1}-\Delta_p) + R_G A_G}{A_G^2+B_G^2}\Omega_p, \quad (13)$$

$$\text{Im}[\tilde{\rho}_{ad}] = \frac{2(\gamma_2+\gamma_2')A_G(\Delta_{o_1}-\Delta_p) - R_G B_G}{A_G^2+B_G^2}\Omega_p. \quad (14)$$

Here, we use the following notations:

$$A_G = -2(\Delta_m-\Delta_p)[(\gamma_1+\gamma_1')(\gamma_2+\gamma_2') + 4\Delta_{o_1}\Delta_p - 4\Delta_p^2 + \Omega_m^2] - 2\Delta_{o_1}\Omega_{o_1}^2 + 2\Delta_p(\Omega_{o_1}^2+\Omega_{o_2}^2) + 2\Omega_{o_1}\Omega_{o_2}\Omega_m\cos\varphi, \quad (15)$$

$$B_G = (\gamma_1+\gamma_1')[4(\Delta_p-\Delta_m)(\Delta_{o_1}-\Delta_p)+\Omega_{o_2}^2] + (\gamma_2+\gamma_2')[4(\Delta_m-\Delta_p)\Delta_p+\Omega_{o_1}^2], \quad (16)$$

$$R_G = 4(\Delta_{o_1}-\Delta_p)(\Delta_p-\Delta_m) + \Omega_{o_2}^2, \quad (17)$$

and introduce a relative phase $\varphi = \varphi_{o_1} + \varphi_{o_2} - \varphi_m$.

Thus, we have derived general expressions for the real and imaginary parts of the density matrix $\tilde{\rho}_{ad}$, that allow us to analyse the optical properties of the ideal four-level atomic scheme displayed in figure 1.

2.2. Doppler broadening

To model an experimental situation we have to take into account the random motion of atoms due to thermal energy. Thermal atomic motion produces a spreading of the absorbed frequency. It results in the broadening of the optical profiles, the so-called Doppler broadening. As a result, for each field i the detuning Δ_i should be replaced by $\Delta_i + k_i v$, where $k_i = \omega_i/c$ is the wave vector of that field. We assume, however, that optical fields have similar transition frequencies

$$k \approx k_{o_1} \approx k_{o_2} \approx k_p. \quad (18)$$

Below we consider a case where the optical, the microwave and the probe fields propagate collinearly along the $+z$ direction. The microwave frequency is much smaller than those of the other driving fields. Therefore, the wave vector of the microwave field can be synchronized with the wave vectors of the optical fields through the two-photon resonance condition as

$$\Delta_m \approx [(\Delta_{o_1}-\Delta_{o_2}) + \beta kv], \quad (19)$$

where $\beta \approx k_m/k$.

Taking into account the above conditions that lead to the velocity-dependent terms: $\Delta_m \to (\Delta_m + \beta kv)$, $\Delta_{o_1} \to (\Delta_{o_1}+kv)$, $\Delta_{o_2} \to (\Delta_{o_2}+kv)$ and $\Delta_p \to (\Delta_p + kv)$, we obtain the following form for the susceptibility

$$\chi(kv) = \frac{N|\wp_{ad}|^2}{\epsilon_0\hbar\Omega_p}[M(kv)\Omega_p], \quad (20)$$

where

$$\begin{aligned} M(kv) &= -\frac{M_1(kv)+M_2(kv)+M_3(kv)}{A_{G_D}^2(kv)+B_{G_D}^2(kv)}, \\ M_1(kv) &= R_{G_D}(kv)A_{G_D}(kv), \\ M_2(kv) &= 2(\gamma_2+\gamma_2')G_{G_D}(kv)B_{G_D}(kv), \\ M_2(kv) &= iQ(kv). \end{aligned} \quad (21)$$

Here,

$$Q(kv) = 2A_{G_D}(kv)G(kv)[(\gamma_2+\gamma_2') - (\Delta_p+kv)] - R_{G_D}(kv)B_{G_D}(kv), \quad (22)$$

$$G_{G_D}(kv) = [\Delta_{o_1} - \Delta_p], \tag{23}$$

and we have obtained the following expressions

$$\begin{aligned} A_{G_D} = &-2[(\Delta_m + \beta kv) - (\Delta_p + kv)] \\ &\times [(\gamma_1 + \gamma_1')(\gamma_2 + \gamma_2') \\ &+ 4(\Delta_{o_1} + kv)(\Delta_p + kv) - 4(\Delta_p + kv)^2 + \Omega_m^2] \\ &- 2(\Delta_{o_1} + kv)\Omega_{o_1}^2 + 2(\Delta_p + kv)(\Omega_{o_1}^2 + \Omega_{o_2}^2) \\ &+ 2\Omega_{o_1}\Omega_{o_2}\Omega_m \cos\varphi, \end{aligned} \tag{24}$$

$$\begin{aligned} B_{G_D} = &4[(\Delta_p + kv) - (\Delta_m + \beta kv)] \\ &\times [(\gamma_1 + \gamma_1')(\Delta_{o_1} - \Delta_p) + (\gamma_2 + \gamma_2')(\Delta_p + kv)] \\ &+ (\gamma_1 + \gamma_1')\Omega_{o_2}^2 + (\gamma_2 + \gamma_2')\Omega_{o_1}^2, \end{aligned} \tag{25}$$

$$R_{G_D} = 4(\Delta_{o_1} - \Delta_p)[(\Delta_p + kv) - (\Delta_m + \beta kv)] + \Omega_2^2. \tag{26}$$

Thus, we obtain for the average susceptibility

$$\chi^{(d)} = \frac{N|\wp_{ad}|^2}{\epsilon_0 \hbar V_D \sqrt{\pi}} \int_{-\infty}^{\infty} M(kv) e^{-\frac{(kv)^2}{V_D^2}} \mathrm{d}(kv), \tag{27}$$

which is defined with the aid of the Maxwell–Boltzmann distribution, where $V_{\mathrm{D}} = \sqrt{k_{\mathrm{B}} T\omega^2/Mc^2}$ is the Doppler width. The Doppler width is a free parameter in our numerical examples. The corresponding group index $N_{\mathrm{g}}^{(d)}$ has the form (2), where χ is replaced by $\chi^{(d)}$. Although we present a general scheme, below a thorough analysis is provided for a resonant interaction as an example, i.e. $\Delta_i = 0$, $i = o_1, o_2, m$.

3. Triplet absorption spectroscopy

To proceed further we separate the susceptibility χ on the imaginary $\Im m\chi \equiv \chi_{\Im}$ and real $\Re e\chi \equiv \chi_{\Re}$ parts

$$\chi_{\Re} = -\frac{N|\wp_{ad}|^2}{\epsilon_0 \hbar \Omega_p} \mathrm{Re}[\tilde{\rho}_{ad}], \tag{28}$$

$$\chi_{\Im} = -\frac{N|\wp_{ad}|^2}{\epsilon_0 \hbar \Omega_p} \mathrm{Im}[\tilde{\rho}_{ad}]. \tag{29}$$

It is convenient to measure the absorption and dispersion in units of $\frac{N|\wp_{ad}|^2}{\epsilon_0 \hbar \Omega_p}$. Most BEC experiments reach quantum degeneracy between 500 nK and 2 μK, at densities between 10^{14} and 10^{15} cm^{-3} [23]. For the number density $N \approx 1.3 \times 10^{14}$ cm^{-3}, $\wp_{ad} = 2.492 \times ea_0$, in the case of the sodium D1 line (a_0 is the Bohr radius) the prefactor $\frac{N|\wp_{ad}|^2}{\epsilon_0 \hbar}$ is about $2\pi \times 9.89$ MHz. This value could be associated with the spontaneous decay rate Γ of the sodium D1 line.

In the analysis below we use $\Gamma \equiv \gamma_1 = \gamma$ as a natural unit of the relevant physical quantities and consider the Rabi frequency of the weak probe field as $\Omega_p = 0.1\gamma$ when $\wp_{ad} = 2.492 \times ea_0$ is chosen for the atomic sodium D1 line. Below some representative examples for the Doppler-free and the Doppler-broadened system are discussed in detail. In this section we consider the value $\varphi = \pi/2$ for the relative phase of the driving fields.

3.1. $\Omega_{o_1} = \Omega_{o_2} = \Omega_m \approx \gamma_1 \gg \gamma_2, \gamma_{1,2}'$

To begin with, we analyse a case that has been studied by many authors in systems with an excited doublet. For example, Knight and co-workers [7] analysed a well-known scheme of a quantum beat laser in the context of spontaneous emission, using the same limit.

Generally, when the intensities of all driving fields are kept comparable to the decay rates $\gamma_{1,2}$, the absorption spectrum splits into a triplet [24, 25]. Note that the triplet is associated with a phenomenon of dynamical Stark triplet splitting. Traditionally it is known as AT splitting.

The positions of the dark lines are determined from the requirement that the numerator of (14) is equal to zero. As a result, one obtains the following estimation

$$\Delta_p \approx \pm\frac{1}{2}\sqrt{\Omega_{o_2}^2 + \gamma_2^2}. \tag{30}$$

These dark lines are due to the quantum interference among three alternative indistinguishable transition pathways to the excited state $|a\rangle$. Qualitatively, this result can be understood from the analysis of the dressed states of three bare pathways: $|d\rangle \to |a\rangle$, $|d\rangle \to |a\rangle \to |b\rangle \to |a\rangle$, $|d\rangle \to |a\rangle \to |c\rangle \to |a\rangle$, coupled by two strong optical fields, and the microwave field. However, this analysis requires a separate study and is beyond the scope of the present paper.

The absorption resonance positions are defined from the requirement $A_G = 0$ (see (15)) that yields three roots. Two of them

$$\Delta_p \approx \pm\frac{1}{2}\sqrt{(\Omega_{o_1}^2 + \Omega_{o_2}^2 + \Omega_m^2) + \gamma_1(\gamma_2 + \gamma_2')} \tag{31}$$

determine the positions of two side peaks, while the central peak is located at $\Delta_p = 0$.

Subsequently, it is easy to estimate each peak height, using the corresponding root. The peak width is evaluated as half of the absorption maximum

$$\frac{\chi_{\Im}}{2} = -\frac{N|\wp_{ad}|^2}{B_G^2 \epsilon_0 \hbar}[(\gamma_2 + \gamma_2')A_G(\Delta_{o_1} - \Delta_p) - R_G B_G)]. \tag{32}$$

at the corresponding root for Δ_p ($\Delta_p = 0$, and see (31)).

The quantum interference generates two dark lines that split the absorption spectra into triplets (see figures 2(a), (d), (g)). At equal intensities of the optical and microwave fields, the width of each component approaches the value $\gamma/3$. As compared with the traditional Λ and Ξ types of systems, here, in addition to the sub-luminal light, the super-luminal light pulse propagates through the three anomalous dispersive windows with some absorption.

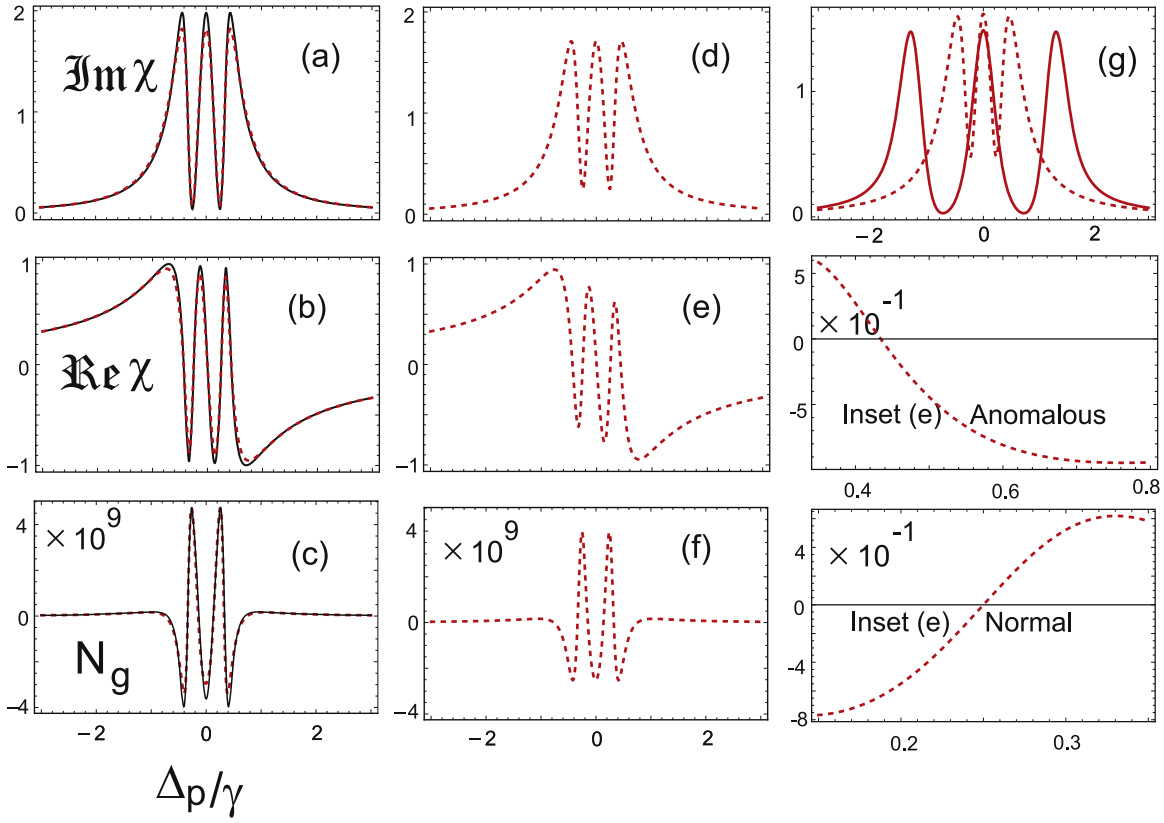

Figure 2. Absorption, dispersion, and group index, versus dimensionless probe field detuning Δ_p/γ. The results at equal intensities $\Omega_{o_1} = \Omega_{o_2} = \Omega_m = 0.5\gamma$ (without and with Doppler broadening; see panels (a), (b), (c)) are connected by solid (black) and dotted (red) lines, respectively. The results at the same intensities (with Doppler broadening and vector mismatch $\beta = 0.5$; see panels (d), (e), (f)) are connected by a dotted (red) line. The results at the vector mismatch $\beta = 0.5$ and at equal-intensity values 0.5γ and 1.5γ are connected by dotted (red) and solid (red) lines, respectively (see panel (g)). On the two right bottom panels the insets for case (e) are displayed. The following parameters are used: $\omega = 10^8\gamma$, $V_D = 0.2\gamma$, $\varphi = \pi/2$, $\gamma_1' = \gamma_2 = \gamma_2' = 0.01\gamma$,

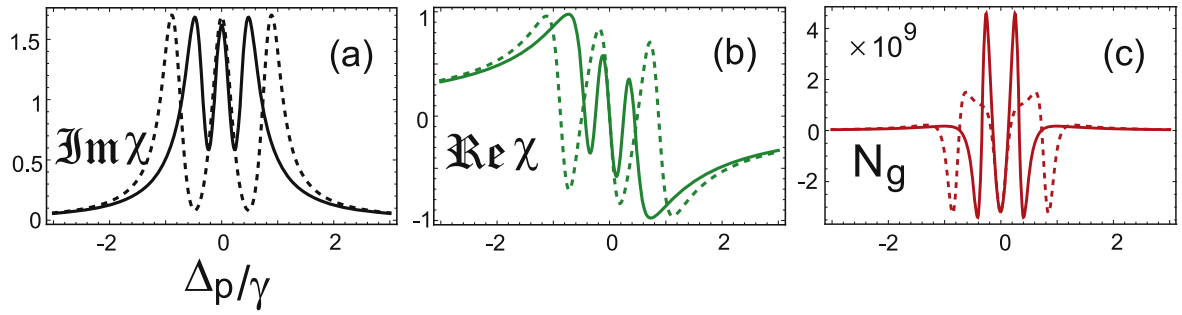

Figure 3. Absorption (a), dispersion (b), and group index (c) versus dimensionless probe field detuning Δ_p/γ at $\beta = 0.5$. The results for $\Omega_{o_1} = \Omega_{o_2} = \Omega_m = 0.5\gamma$, and $=\gamma$ are connected by solid and dashed lines, respectively. The other parameters are kept the same as in figure 2.

Thus, at equal intensities of the driving fields, there is a dominance of the sub-luminal light over the super-luminal one (see figure 2(c)). This dominance can be explained in simple terms. In the insets of figure 2(e) we zoom the right wing of the dispersion $\Re e\chi$. Evidently, it is related to the absorption spectrum via the Kramers–Kronig relation. While the anomalous dispersion decreases exponentially with the increase of the ratio Δ_p/γ, the normal dispersion grows faster with the increase of this ratio.

The sub-luminality and super-luminality are affected by the vector mismatch. The vector mismatch βk degrades the interference, especially the super-luminality (compare figures 2(c), (f)). The increase of the intensity increases the EIT windows (see figure 2(g)). However, this increase yields: i) a decrease in the steepness of the transparency windows; and ii) a widening of the absorption spectrum. In addition, it leads to the attenuation of the sub-luminality of the system (see figure 3). Note, however, that the super-luminality is much less affected.

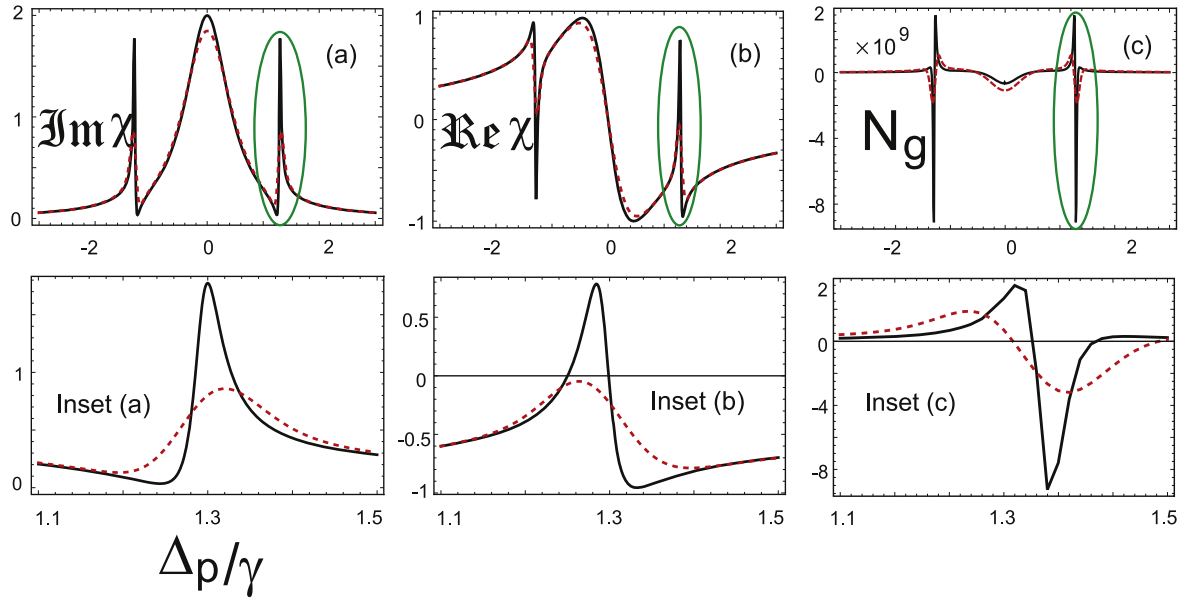

Figure 4. Top row: absorption (a), dispersion (b), and group index (c) versus dimensionless probe field detuning Δ_p/γ. Bottom row: the insets for cases (a)–(c) are displayed. The following parameters are chosen: $\Omega_{o_1} = \Omega_m = 0.5\gamma$ and $\Omega_{o_2} = 2.5\gamma$. The results at $\beta = 0$, 0.5 are connected with solid (black) and dashed (red) lines, respectively. The other parameters are kept the same as in figure 2.

3.2. $\Omega_{o_2} > \Omega_{o_1} = \Omega_m, \gamma_1 \gg \gamma_2, \gamma'_{1,2}$

At the Doppler-free case, it is convenient to estimate analytically the locations of: (i) two dark lines; (ii) three spectral components; and (iii) their widths. By means of the same recipe (see section 3.1), we obtain for the dark line positions

$$\Delta_p \approx \pm\frac{1}{2}\sqrt{\Omega_{o_2}^2 + \gamma_2^2}. \tag{33}$$

In this case the locations of side absorption resonances are determined by (31). Similar to the results of section 3.1, the central peak is located at $\Delta_p = 0$. In the considered conditions, (32) can still be useful to define the absorption resonance widths. Note that these estimations agree with the corresponding results obtained numerically in the presence of Doppler broadening and vector mismatch.

The dominance of the optical fields with respect to the other driving fields leads to the broadening of the central peak, while the side resonance widths are decreasing. In this case the quantum interference of three resonances produces a pattern that is typical for the Fano-like interference phenomenon [19]. The Lorentzian shape of the central peak is complemented by two side resonances with asymmetric shapes (see figure 4(a)).

The super-luminal behaviour of the pulse around the two side windows with anomalous dispersions is significantly enhanced, when the intensity of the optical field Ω_{o_2} relative to the other driving fields is kept high (see figure 4(c)). On the other hand, the sub-luminality at the two side windows with normal dispersion worsens. The largeness and smallness of the positive (negative) group index is correlated through steepness and flatness in the normal (anomalous) dispersion (compare figures 2(e) and 4(b)).

Thus, the vector mismatch of the microwave field with the other driving fields degrades the interference. The larger the value of the parameter β, the greater the degradation. Although the vector mismatch strongly attenuates the superluminality in the side transparency windows, the attenuation is much weaker in the central transparency window (see figure 4(a)). At high strength of the optical field Ω_{o_2} the rate of atomic oscillations between the second ground state and the excited state is fast as compared with the decay rates of the states of the excited doublet. Therefore, the quantum interference is more effective due to the decrease in decay rates. However, the inherited incoherence, produced by the vector mismatch of the microwave field, may require higher optical field intensity for its suppression.

4. Simplistic triplet absorption spectroscopy

4.1. One decay channel

The question arises: is it possible to simulate a physical situation where incoherent processes, discussed above, can be avoided? Fortunately, this can happen in a scheme based on a simple probability loss, where the contribution of decoherence due to the vector mismatch is relaxed.

Let us consider the sodium atom in a weak static magnetic field, where there is only one decay channel. Evidently, Zeeman splitting yields families of states with different magnetic quantum numbers m (see figure 5). The microwave field with frequency ω_m couples a low-lying state $|b\rangle$ and a ground state $|c\rangle$ with the Rabi frequency Ω_m. These two states are coupled with the excited state $|a\rangle$ by the two optical fields of frequencies ω_{o_1} and ω_{o_2} with the corresponding Rabi frequencies Ω_{o_1} and Ω_{o_2}, to form a loop. A weak

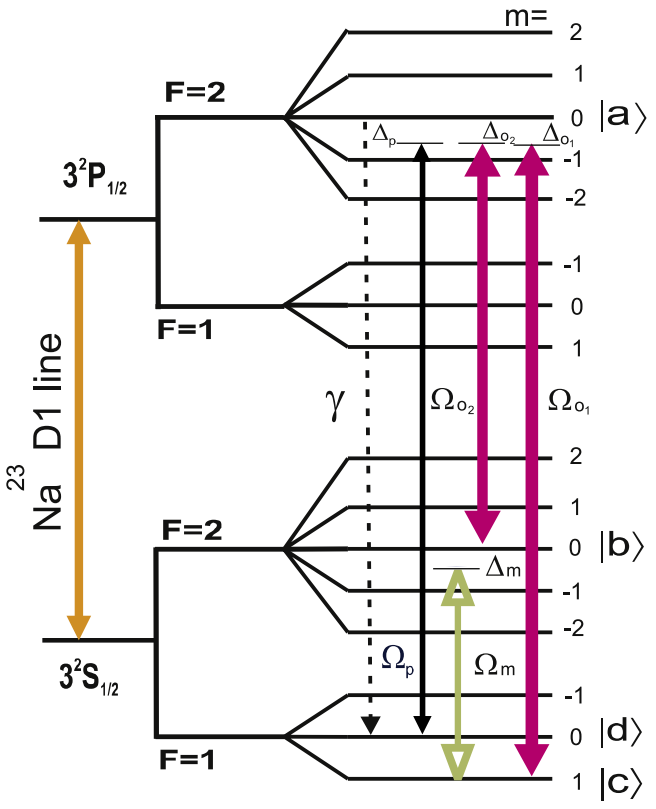

Figure 5. A sketch of the atomic energy spectrum of the sodium D1 line at a weak magnetic field.

probe field couples the excited state $|a\rangle$ with a low-lying state $|d\rangle$. The simplicity in the radiative decay process in the present scheme (observed experimentally [26]) provides the proper ground to study the interplay between the driving fields at a small decoherence background created by the one decay channel.

This simplistic system is described by the Hamiltonian (taken in the interaction representation and in the rotating wave approximation)

$$H_I = -\frac{\hbar}{2}[\Omega_m e^{i(\Delta_m t+\varphi_m)}|b\rangle\langle c| + \Omega_{o_1} e^{i(\Delta_{o_1} t+\varphi_{o_1})}|a\rangle\langle c| + \Omega_{o_2} e^{i(\Delta_{o_2} t+\varphi_{o_2})}|a\rangle\langle b| + \Omega_p e^{i\Delta_p t}|a\rangle\langle d|] + \text{H.c.} \tag{34}$$

Applying our approach (see section 2) to the Hamiltonian (34), we obtain for the real and imaginary parts of the susceptibility

$$\chi_{\Re} = -\frac{N|\wp_{ad}|^2}{\epsilon_0\hbar\Omega_p}\left[\frac{R_S A_S}{A_S^2 + B_S^2}\Omega_p\right], \tag{35}$$

and

$$\chi_{\Im} = +\frac{N|\wp_{ad}|^2}{\epsilon_0\hbar\Omega_p}\left[\frac{R_S B_S}{A_S^2 + B_S^2}\Omega_p\right]. \tag{36}$$

Here

$$\begin{aligned} A_S &= 2(\Delta_{o_2} - \Delta_p)[4\Delta_p(\Delta_p - \Delta_{o_1}) - \Omega_{o_2}^2] - 2\Delta_{o_1}\Omega_{o_1}^2 \\ &\quad + 2\Delta_p(\Omega_{o_1}^2 + \Omega_m^2) + 2\Omega_{o_1}\Omega_{o_2}\Omega_m\cos\varphi, \\ B_S &= 4\gamma(\Delta_p - \Delta_{o_2})(\Delta_{o_1} - \Delta_p) + \gamma\Omega_m^2, \\ R_S &= 4(\Delta_{o_1} - \Delta_p)(\Delta_p - \Delta_{o_2}) + \Omega_m^2, \end{aligned} \tag{37}$$

where $\varphi = \varphi_m + \varphi_{o_1} - \varphi_{o_2}$

Note, that for the Doppler-free system, at the resonance condition $\Delta_{o_1} = \Delta_{o_2} = 0$, the absorption is cancelled if the equation

$$\Delta_p = \pm\frac{1}{2}\Omega_m \tag{38}$$

is fulfilled, since $B_S = 0$. Two dark lines are developed in the Lorentzian-type absorption spectrum irrespective of the decay rate and the intensities of the optical fields. However, it is controlled by the intensity of the microwave field. The positions of the central absorption and the side absorption peaks (components) of the triplet are located at the roots $\Delta_p = 0$ and

$$\Delta_p = \pm\frac{1}{2}\sqrt{\Omega_{o_1}^2 + \Omega_{o_2}^2 + \Omega_m^2}, \tag{39}$$

respectively, when $A_S = 0$ at $\varphi = \pi/2$. The width of each spectral component can be easily evaluated by means of the equation

$$\chi_{\Im}/2 = -\frac{N|\wp_{ad}|^2}{\epsilon_0\hbar B_S}, \tag{40}$$

where Δ_p in the expression for B_S (see (37)) is replaced either by zero or by the corresponding root of (39).

Thus, we have derived the system of equations that define the real and imaginary terms of the susceptibility in an ideal case of the one decay channel. As before, a thorough analysis is provided for a resonant interaction as an example, i.e. $\Delta_i = 0$, $i = o_1, o_2, m$.

4.2. Doppler broadening and vector mismatch

To trace the influence of the Doppler broadening, we consider the collinear propagation of the microwave field, the two optical fields and the probe fields. This consideration yields the replacements of $\Delta_m \to (\Delta_m + \beta kv)$, $\Delta_{o_1} \to (\Delta_{o_1} + kv)$, $\Delta_{o_2} \to (\Delta_{o_2} + kv)$ and $\Delta_p \to (\Delta_p + kv)$ in (35), (36). The synchronization of the microwave field with the optical driving fields requires the condition $\Delta_{o_2} = (\Delta_{o_1} - \Delta_m)$ to be fulfilled (the two-photon Raman resonance condition).

Taking into account the vector mismatch $\Delta_m \to (\Delta_m + \beta kv)$, we use the substitution $\Delta_{o_2} \to [(\Delta_{o_1} - \Delta_m) + (1 - \beta)kv]$ in (35)–(37), in addition to the substitution of the other velocity-dependent terms. The average susceptibility is defined as before

$$\chi(kv) = \frac{N|\wp_{ad}|^2}{\epsilon_0\hbar\Omega_p}\left[\frac{R_{S_D}(kv)A_{S_D}(kv) + iQ_{S_D}(kv)}{A_{S_D}^2(kv) + B_{S_D}^2(kv)}\Omega_p\right], \tag{41}$$

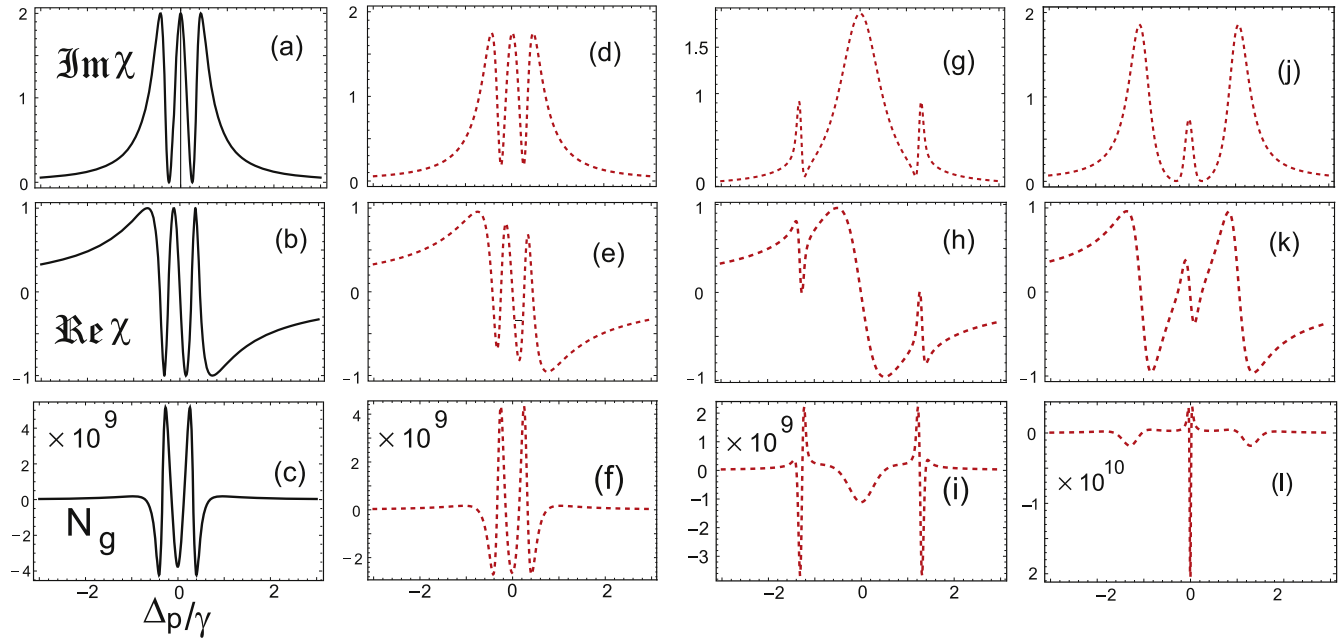

Figure 6. Absorption (a), (d), (g), (j), dispersion (b), (e), (h), (k), and group index (c), (f), (i), (l), versus the field detuning, Δ_p/γ. The following parameters are used: $\omega = 10^8\gamma$, $V_D = 0.2\gamma$, $\varphi = \pi/2$. The results for equal intensities $\Omega_{o_1} = \Omega_{o_2} = \Omega_m = 0.5\gamma$ are connected by a solid (black) line for $\beta = 0$ (a)–(c), and a dashed (red) line for $\beta = 0.5$ (d)–(f). The results for $\Omega_m = 2.5\gamma$, $\Omega_{o_1} = \Omega_{o_2} = 0.5\gamma$, and $\beta = 0.5$ are connected by a dashed (red) line (g)–(i). The results for $\Omega_{o_2} = \Omega_m = 0.5\gamma$, $\Omega_{o_1} = 2.5\gamma$ are connected by a dashed (red) line for $\beta = 0.5$ (j)–(l).

where

$$A_{S_D}(kv) = -2(\Delta_{o_1} + kv)\Omega_{o_1}^2 + 2(\Delta_p + kv)(\Omega_{o_1}^2 + \Omega_m^2) + 2[[(\Delta_{o_1} - \Delta_m) + (1-\beta)kv] - (\Delta_p + kv)] \times [4(\Delta_p + kv)(\Delta_p - \Delta_{o_1}) - \Omega_{o_2}^2] + 2\Omega_{o_1}\Omega_{o_2}\Omega_m \cos\varphi, \tag{42}$$

$$B_{S_D}(kv) = \gamma\Omega_m^2 + 4\gamma(\Delta_{o_1} - \Delta_p) \times [(\Delta_p + kv) - [(\Delta_{o_1} - \Delta_m) + (1-\beta)kv]], \tag{43}$$

$$R_{S_D}(kv) = \Omega_m^2 + 4(\Delta_{o_1} - \Delta_p) \times [(\Delta_p + kv) - [(\Delta_{o_1} - \Delta_m) + (1-\beta)kv]], \tag{44}$$

$$Q_{S_D}(kv) = -2A_{S_D}(kv)B_{S_D}(kv)R_{S_D}(kv). \tag{45}$$

In this system the quantum interference is always dominant for both the Doppler-free and Doppler-broadened cases due to simple losses. In fact, this is a nice manifestation of the Fano-like interference mechanism in triplet spectroscopy. In the case of doublet spectroscopy, at the resonance condition, the position of the dark line is always fixed (see e.g. [1, 17]). In our model there are two dark lines in the absorption spectra, independently of the strength of the driving fields at the relative phase $\varphi = \pi/2$ (see top row of figure 6). Their positions can be changed by the intensity of the microwave field (see (38)). In virtue of this fact, one can tune up the whole system by a proper choice of the optical fields.

Evidently, the Doppler broadening degrades the system coherence. In addition, the vector mismatch relaxes the sub- and super-luminality (compare figures 6(a)–(c) and figures 6(d)–(f)) at the equal intensity of the driving fields. However, as shown in section 3.2, one can control the properties of the central absorption peak by choosing the appropriate optical field to be dominant over other parameters of the system. In fact, many features are simply the consequence of the Kramers–Kronig relations. Two side peaks and a small central peak in the absorption spectrum correspond to anomalous dispersions for the probe field. The dominance of the intensity of the optical field Ω_{o_1} yields a drastic increase of the super-luminality (compare figures 6(f), (l)) and the attenuation of the sub-luminality of the side peaks.

At the dominance of the microwave field Ω_m, for the central broadened peak (see figure 6(g)) the dispersion is mild (see figure 6(h)). The substantial enhancement in the group index for the steep anomalous regions at the side positions of the absorption spectra is accompanied by the attenuation of the super-luminality at the central position due to the flattened dispersion (compare figures 6(f), (i)).

Thus, in the proposed scheme one is able to control the transparency windows by means of the external fields in triplet absorption spectroscopy. The EIT aspect related to the absorption/dispersion properties of the proposed scheme is studied in detail below.

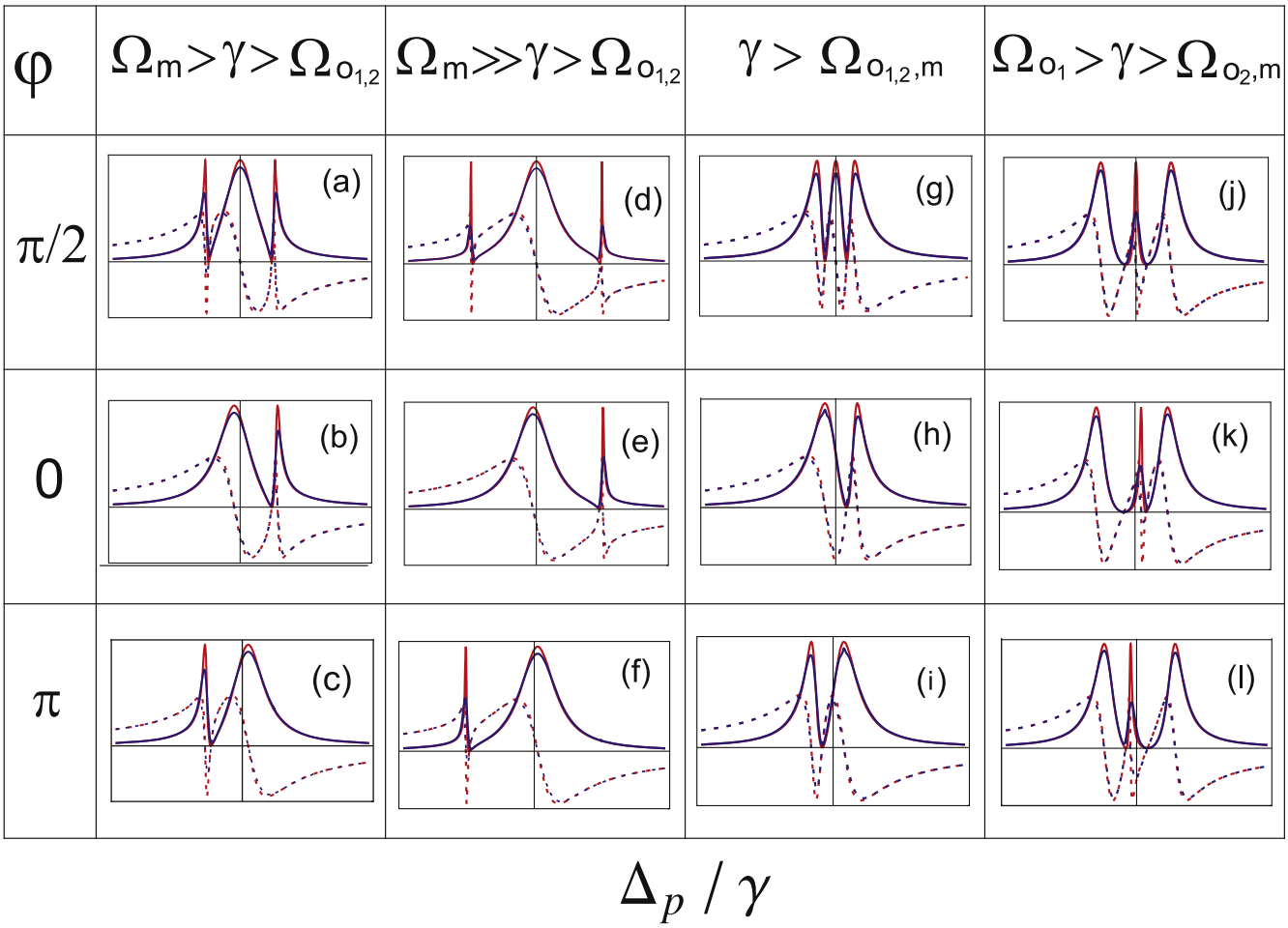

Figure 7. Absorption (solid line) and dispersion (dashed line) versus dimensionless probe field detuning Δ_p/γ. The red lines connect the results without Doppler broadening and vector mismatch; the blue lines connect the results with vector mismatch $\beta k = 0.5\gamma$ and Doppler width $V_D = 0.2\gamma$. Panels (a), (b), (c): $\Omega_{o_1} = \Omega_{o_2} = 0.5\gamma$, $\Omega_m = 1.5\gamma$. Panels (d), (e), (f): $\Omega_{o_1} = \Omega_{o_2} = 0.5\gamma$, $\Omega_m = 3\gamma$. Panels (g), (h), (i): $\Omega_{o_1} = \Omega_m = \Omega_{o_2} = 0.5\gamma$. Panels (j), (k), (l): $\Omega_m = \Omega_{o_2} = 0.5\gamma$, $\Omega_{o_1} = 1.5\gamma$. The other parameters are kept the same as in figure 6.

4.3. Control of the EIT windows

To understand better the quantum interference phenomenon we consider different relative phases $\varphi = 0, \pi/2, \pi$ of the driving fields. Note that the results for the phase values $\varphi = 0, \pi/2$ represent a mirror reflection of those obtained for the values $\varphi = \pi, 3\pi/2$. We summarize our findings in figure 7, which are also consistent with the results of section 3.

Obviously, the spectrum is split into a triplet by two dark lines developed in the Lorentzian-type absorption spectrum at $\Delta_p = \pm\Omega_m/2$ (see figure 7(g) for $\varphi = \pi/2$). The width of each spectral component appears as $\gamma/3$ when the intensities of the driving fields are kept equal. The quantum interference is always dominant for the Doppler-free and Doppler-broadened cases, due to the simple probability loss. The absence of additional radiative decay rates in the system relaxes the influence of the vector mismatch of the microwave field. However, if the microwave field is switched off, control of the EIT is reduced, since one is faced with the traditional tripod systems (see, e.g., [27]).

Double transparency windows could exist in the system as well if one of the optical fields is switched off. In this case, the absorption (35) and dispersion (36) spectra become phase insensitive, when either Ω_{o_1} or Ω_{o_1} is set to zero in (42). Therefore, to maintain phase effects in the system, it is important to preserve the loop structure couplings of the driving fields.

To illuminate the crucial role of the microwave field and the relative phase of the driving fields, we neglect the effect of the Doppler broadening and focus on the absorption (36) at the resonance condition $\Delta_{o_2} = \Delta_{o_1} = \Delta_m = 0$. In this case we have

$$A_{S_R} = -8\Delta_p^3 + 2\Omega^2\Delta_p + 2\Omega_{o_1}\Omega_{o_2}\Omega_m \cos\varphi, \tag{46}$$

$$R_{S_R} = \Omega_m^2 - 4\Delta_p^2, \quad B_{S_R} = \gamma R_{S_R}, \tag{47}$$

$$\Omega^2 = \Omega_{o_1}^2 + \Omega_{o_2}^2 + \Omega_m^2. \tag{48}$$

We recall that the prefactor $N|\wp_{ad}|^2/(\epsilon_0\hbar) \equiv \gamma$ is our natural unit. Further, for the sake of convenience we introduce the

following notations

$$y_i = \Omega_i/2\gamma, \quad i = o_1, o_2, m, \quad x = \Delta_p/\gamma. \tag{49}$$

Taking into account these definitions, it is straightforward to present (36) in the Fano-type form

$$\chi_\Im = \frac{(x^2 - y_m^2)^2}{4F^2 + (x^2 - y_m^2)^2}, \tag{50}$$

$$F = x^3 - K^2 x - M\cos\varphi, \tag{51}$$

$$K^2 = (y_1^2 + y_2^2 + y_m^2), \quad M = 2y_1 y_2 y_m. \tag{52}$$

These equations demonstrate clearly the dependence of the absorption on the strength of the microwave field and the relative phase φ of the driving fields. It appears that the positions of the dark lines are always determined as $x = \pm y_m \Rightarrow \Delta_p = \pm\Omega_p/2$. However, this result should be taken cautiously, since the phase factor plays an important role as well.

Evidently, the roots of (51) determine the position of three absorption maxima (see figures 7(a), (d), (g), (j)) in general. In particular, at $\varphi = \pi/2$ they are defined by (38, 39). There is, however, a significant influence of the relative phase of the driving fields on the tunability of the Fano-like resonances in the triplet absorption spectrum. Two Fano-like resonances can be tuned into a single Fano-like resonance and vice versa in the absorption spectrum if the relative phase of the driving fields is varied.

Indeed, the central absorption peak (see figures 7(a), (d), (g)) merges: either with its left (right) peak at the phase $\varphi = 0$ ($\varphi = \pi$) in figures 7(b), (e), (figures 7(c), (f)), or with its right (left) peak in figure 7(h) (figure 7(i)). As an example, we consider the case of figure 7(b): $\Omega_{o_1} = \Omega_{o_2} = 0.5\gamma$, $\Omega_m = 1.5\gamma$, $\varphi = 0$. By means of (49, 50, 51, 52), one readily obtains

$$\chi_\Im = \frac{(x^2 - 9/16)^2}{4(x + 3/4)^2[(x - 3/8)^2 - 17/64]^2 + (x^2 - 9/16)^2} = \frac{(x - 3/4)^2}{4[(x - 3/8)^2 - 17/64]^2 + (x - 3/4)^2}. \tag{53}$$

The position of only one dark line is located at $x = 3/4$, while two absorption maxima are determined by $x_{1,2} = 3/8 \pm \sqrt{17}/8$. In this process, one of the Fano-like resonances (and dark lines) disappears from the spectrum. The width of the merged peak is compensated by the increase of the width of the corresponding side peak. In addition, for a high relative strength, the central broadened peak is merged with the side one (see figures 7(e), (f)).

Unlike the study in [28], where the Fano-like resonance was tuned by using some approximation in the opto-mechanics set-up, here control of the single dynamical variable φ is enough to control the resonance profile.

Depending on the phase and relative intensities of the driving fields, the dispersion associated with the central and side components of the absorption spectrum superimposes at the cost of large absorption developed by the merging effect. Subsequently, we are left with one EIT window on either side of the central line (see figures 7(b), (e), (h) and figures 7(c), (f), (i)). As a result, the height and the width of the absorption peak will increase, and the sub-luminal light is converted to a super-luminal one. We expect that the probe pulse would be greatly attenuated during the propagation through the transparency window with the anomalous dispersion.

Thus, phase control can be used to convert the double transparency behaviour of the medium to a single transparency one and vice versa. In addition, at the dominance of the optical fields, we obtain a shift of the central peak either to the left ($\phi = 0$) or to the right ($\phi = \pi$) side with respect to its position at ($\phi = \pi/2$) (see figures 7(j), (k), (l)).

Note that the dark line positions with and without vector mismatch are controlled by the intensity of the microwave field Ω_m (see figures 7(a), (d)) as well. The higher the intensity of the microwave field, the wider the transparency windows, with a similar mirror inversion for the dispersions. The sharper and shorter anomalous dispersions associated with the two sides' sharp absorption lines are now away from the central location of the spectrum. Therefore, the sub-luminal probe pulse propagation through the two windows is degraded. However, once the intensity of the optical field —Ω_{o_1}, Ω_{o_2}, or both—is increased, the normal dispersions worsen at the two windows. Subsequently, the central absorption line becomes extremely narrowed with a giant anomalous dispersion. In response, the slow light through the transparency window becomes extremely degraded (see figures 7(j), (k), (l)).

We conclude that the widths of the three components of the triplet spectrum are not dependent on the frequencies of two optical and microwave fields. We recall that in the traditional one-window based EIT systems the widths of the absorption components of the corresponding spectrum are independent of the intensities of the control fields. However, in the considered system the widths depend on their intensities and their coupling positions in the interaction loop relative to the decaying energy level. For example, the width of the central component in the considered simplistic scheme is narrowed with the increase of the intensity of the optical field ω_{o_1} or the optical field ω_{o_2}, or both of them. On the other hand, the microwave field, coupled indirectly to the decaying energy level, produces the opposite effect. Namely, the width of the central peak is broadened with the increase of the microwave field intensity. In addition, manipulation of the EIT windows is achieved by means of an effective tuning of the microwave field intensity.

5. Summary

We have analysed thoroughly the coherence phenomena produced by three cyclically driven optical fields in four-level systems at zero and weak magnetic fields. To this end we have developed a model in order to trace the optical response of the atomic sodium system, as an example. It was found that in this system the coherence effects yield two dark lines, in general. This is due to the EIT phenomenon which manifests the interplay between the AT and the Fano-like mechanisms in triplet absorption spectroscopy.

To gain a better insight into the coherence phenomena we have proposed the ideal but experimentally viable behaviour of our system at a weak magnetic field. We have provided various sets of parameters to explore the transition from a multiple broad-band window to extremely narrow-band windows for transparency of the probe pulse. Such effect could exist only when two optical fields are coupled in a combination with a microwave field to form a loop structured interaction. In fact, we found a significant influence of the relative phase of the driving fields on the tunability of the Fano-like resonances in the triplet absorption spectrum. Two Fano-like resonances in the absorption spectrum can be tuned into a single Fano-like resonance and vice versa. We have demonstrated that the degree of EIT (with and without Doppler broadening) can be controlled by altering the intensities of the external optical fields as well.

We speculate that the controllability of the EIT windows by means of manipulation of the intensity of the microwave field and the relative phase of the driving fields in the considered system could help to improve some technical aspects of devices already in use or yet to be developed [17]. In particular, the coherence and interference phenomena, similar to the EIT in gaseous media and optoelectronic materials [17, 29], show promise for some logic and functional operations such as NOT and AND gates when a system enables the production of enhanced double EIT [30].

From our calculations it follows that the normal dispersions around the two dark lines are extremely flattened. As a result, the sub-luminality is attenuated (see figures 6(j), (k), (l)). As a matter of fact, it is the microwave field that enables one to control the positions of the dark lines in triplet spectroscopy, and, subsequently, to change the sub- and super-luminality of the probe pulse.

Steep anomalous dispersions at the corresponding windows are accompanied by a relatively small but sharp absorption. It results in a drastic enhancement of the superluminal group velocity of the probe pulse. The enhanced group velocity of light promises various experimental applications. For example, the quality of an image measured by a light pulse with a relatively low group velocity could be improved if measured by a super-luminal light pulse with a significantly high group velocity [31].

Acknowledgements

F G is grateful for the warm hospitality at JINR. This work was supported in part by the Russian Foundation for Basic Research, Grant 14-02-00723, and by COMSATS Institute of Information Technology, Islamabad.

References

[1] Scully M O and Zubairy M S 1997 *Quantum Optics* (Cambridge: Cambridge University Press)
[2] Autler S H and Townes C H 1955 *Phys. Rev.* **100** 703
Knight P L and Milonni P W 1980 *Phys. Rep.* **66** 23
[3] Fano U 1961 *Phys. Rev.* **124** 1866
Fano U and Cooper J W 1968 *Rev. Mod. Phys.* **441** 50
[4] Agarwal G S 1991 *Phys. Rev.* A **44** R28
Wang D and Zheng Y 2011 *Phys. Rev.* A **83** 013810
[5] Agassi D 1984 *Phys. Rev.* A **30** 2449
[6] Zhu S Y, Narducci L M and Scully M O 1995 *Phys. Rev.* A **52** 4791
[7] Paspalakis E, Keitel C H and Knight P L 1998 *Phys. Rev.* A **58** 4868
[8] Cahuzac P and Vetter R 1976 *Phys. Rev.* A **14** 270
[9] Bjorkholm J E and Liao P F 1977 *Opt. Commun.* **21** 132
[10] Gray H R and Stroud C R Jr 1978 *Opt. Commun.* **25** 359
[11] Delsart C, Keller J C and Kaftandjian V P 1981 *J. Phys.* **42** 529
[12] Fisk P T H, Bachor H A and Sandeman R J 1986 *Phys. Rev.* A **33** 2418
[13] Zhang Y, Anderson B and Xiao M 2008 *J. Phys. B: At. Mol. Opt. Phys.* **41** 045502
[14] Nie Z, Li H Z P, Yang Y, Zhang Y and Xiao M 2008 *Phys. Rev.* A **77** 063829
[15] Du Y *et al* 2009 *Phys. Rev.* A **79** 063839
[16] Zhang Y, Li P, Zheng H, Wang Z, Chen H, Li C, Zhang R and Xiao M 2011 *Opt. Express* **19** 7769
[17] Fleischhhauer M, Imamoglu A and Marangos J P 2005 *Rev. Mod. Phys.* **77** 633
[18] Bhattacharyya D, Ray B and Ghosh P N 2007 *J. Phys. B: At. Mol. Opt. Phys.* **40** 4061
Li S, Yang X, Cao X, Xie C and Wang H 2007 *J. Phys. B: At. Mol. Opt. Phys.* **40** 3211
Li H, Sautenkov V A, Rostovtsev Y V, Welch G R, Hemmer P R and Scully M O 2009 *Phys. Rev.* A **80** 023820
[19] Miroshnichenko A E, Flach S and Kivshar Y S 2010 *Rev. Mod. Phys.* **82** 2257
[20] Knight P L, Lauder M A and Dalton B J 1990 *Phys. Rep.* **190** 1
[21] Novikova I, Walsworth R L and Xiao Y 2012 *Laser Photonics Rev.* **6** 333
[22] Wang C L, Li A J, Zhou X Y, Kang Z H, Jiang Y and Gao J Y 2008 *Opt. Lett.* **33** 687
Shen J Q and Zhang P 2007 *Opt. Express* **15** 6484
[23] Ketterle W 2002 *Rev. Mod. Phys.* **74** 1131
[24] Sahrai M, Tajali H, Kapale K T and Zubairy M S 2006 *Phys. Rev.* A **73** 023813
[25] Zhu S Y and Scully M O 1996 *Phys. Rev. Lett.* **76** 388
Paspalakis E and Knight P L 1998 *Phys. Rev. Lett.* **81** 293
Ghafoor F, Zhu S Y and Zubairy M S 2000 *Phys. Rev.* A **62** 013811
[26] Kuo-cheng C 2000 *PhD Thesis* The University of Texas at Dallas
[27] Alotaibi H M M and Sanders B C 2015 *Phys. Rev.* A **91** 043817
[28] Akram M J, Ghafoor F and Saif F 2015 *J. Phys. B: At. Mol. Opt. Phys.* **48** 065502
[29] Hau L V, Harris S E, Dutton Z and Behroozi C H 1999 *Nature* **397** 594
Bolda E L, Garrison J C and Chiao R Y 1994 *Phys. Rev.* A **49** 2938
[30] Shen J Q and Zhang P 2007 *Opt. Express* **15** 6484
[31] Glasser R T, Vogl U and Lett P D 2012 *Opt. Express* **20** 13702